

Volumetric multiple optical traps produced by Devil's lenses

Walter D. Furlan

walter.furlan@uv.es

Fernando Giménez

Arnau Calatayud

Laura Remón

Juan A. Monsoriu

Departamento de Óptica, Universitat de València, E-46100 Burjassot, Spain

Instituto de Matemática Pura y Aplicada, Universidad Politécnica de Valencia, E-46022, Valencia, Spain

Centro de Tecnologías Físicas, Universidad Politécnica de Valencia, E-46022 Valencia, Spain

Centro de Tecnologías Físicas, Universidad Politécnica de Valencia, E-46022 Valencia, Spain

Centro de Tecnologías Físicas, Universidad Politécnica de Valencia, E-46022 Valencia, Spain

We propose the use of a new diffractive optical element coined Devil's Vortex-Lens (DVL) to produce optical tweezers. In its more general form it results as the combination of a Devil's lens and a helical vortex phase mask. It is shown that under monochromatic illumination a DVL generates a focal volume with several concatenated doughnut modes that are axially distributed according to the self-similarity of the lens. The orbital angular momentum associated to each link in the chain is investigated. [DOI: 10.2971/jeos.2010.100375]

Keywords: optical trapping, optical vortices, vortex lenses

1 INTRODUCTION

Optical vortices extended the capabilities of conventional optical traps because in addition to trap microparticles they are capable to set these particles into rotation due to its inherent orbital angular momentum [1, 2]. In this way, optical vortices are proposed a promising class of actuators for micromechanical systems [3], and arrays of optical vortices have shown the ability to assemble colloidal particles into mesoscopic pumps for microfluidic systems [4].

Among the several methods that have been proposed for optical vortices generation the spiral phase plate [5] stands out, mainly because it provides high energy efficiency. Spiral phase plates have been recently combined with other novel optical elements, the Fractal zone plates (FraZPs), to produce a sequence of focused optical vortices along the propagation direction. Two different results were independently obtained: the *spiral fractal zone plate* [6] and the *devil's vortex lens* [7]. The later has been shown to have even better diffraction efficiency than the former.

It has been demonstrated that, these vortex lenses provide the potential to generate multiple-plane optical trappings in the microscopic scale with a true volumetric extension. This feature represents an advantage over conventional vortices, since they are not maintained as focused outside the depth of focus of the beam. Since the DVL improves the diffraction efficiency of the spiral fractal zone plate; in this paper, we emphasize that these elements are able to create a chain of optical traps along the optical axis with a tunable separation, strength and transverse section. Further, we develop some additional

properties of DVL. We discuss the influence of the topological charge on the self-similarity of the axial irradiance and also we investigate the variation of the angular momentum provided by the doughnut shaped foci.

2 LENSES WITH DEVIL'S STAIRCASE PROFILE.

Fractal zone plates (FraZP) are zone plates with a fractal structure along the squared radial coordinate [8]–[11]. Compared with a binary Fresnel zone plate, a FraZP presents not only the major foci appearing at distances of $f, f/3, f/5, \dots$, but also several additional subsidiary focal points surrounding the regions of the axial major foci. The axial distribution of these foci follows the fractal structure of the FraZP. Inspired by the FraZP we have recently presented the DVL which are pure phase blazed FraZPs modulated by a helical phase structure [7].

The design of a DVL is based on the 1-D Cantor function [11, 12] also known as *devil's staircase*. This function is defined in the domain $[0,1]$ as

$$F_S(x) = \begin{cases} \frac{l}{2^S} & \text{if } p_{S,l} \leq x \leq q_{S,l} \\ \frac{1}{2^S} \frac{x - q_{S,l}}{p_{S,l+1} - q_{S,l}} + \frac{l}{2^S} & \text{if } q_{S,l} \leq x \leq p_{S,l+1} \end{cases}, \quad (1)$$

being $F_S(0) = 0$ and $F_S(1) = 1$. In Figure 1 we have represented the triadic Cantor set developed up to $S = 3$ and the corresponding function $F_3(x)$. It can be seen that the steps of the devil's staircase, take the constant values $l/2^3$ in the inter-

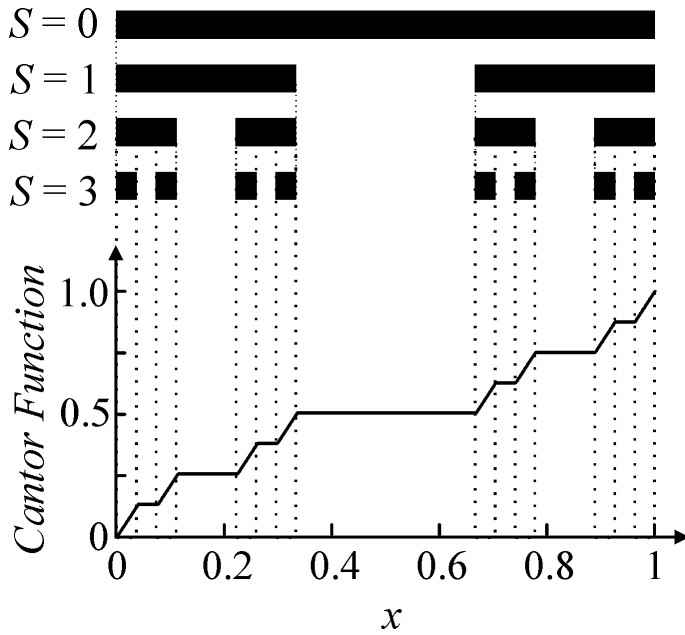


FIG. 1 Triadic Cantor set for $S = 1, 2,$ and 3 . The structure for $S = 0$ is the initiator and the one corresponding to $S = 1$ is the generator. The Cantor function or Devil's staircase, $F_S(x)$, is shown under the corresponding Cantor set for $S = 3$.

vals $p_{3,l} \leq x \leq q_{3,l}$ (with $l = 1, \dots, 7$) whereas in between these intervals the function increases linearly.

From a particular Cantor function $F_S(x)$ a DVL is a pure-phase diffractive optical element whose transmittance is defined by

$$q(\zeta, \varphi) = \exp \left[-i2^{S+1} \pi F_S(\zeta) \right] \times \exp [im\varphi], \quad (2)$$

where $\zeta = (r/a)^2$ is the normalized quadratic radial variable, a is the lens radius, and m is the topological charge. Thus the transmittance of a DVL can be expressed as the product of two factors, the first one, associated to a devil's lens [11], has only a radial dependence. The other one, corresponds to a vortex lens and it has a linear phase dependence on the azimuthal angle. Note that, the phase variation along the radial coordinate is quadratic in each zone of the lens. At the gap regions defined by the Cantor set the phase shift is $-l2\pi$, with $l = 1, \dots, 2^S - 1$. The form of DVLs for $S = 3$ and for several values of the topological charge $m = 0, 1, 2$ are depicted in the right column of Figure 2 in which the gray levels show the continuous phase variation. For comparison, the corresponding conventional kinoform vortex lenses are shown in the left column of the same figure.

3 AXIAL BEHAVIOR OF DVLs.

Within the Fresnel approximation the diffracted field at a given point (z, r, θ) can be characterized by the irradiance and the phase functions, which are given respectively by:

$$I(z, r) = \left(\frac{2\pi}{\lambda z} \right)^2 \left| \int_0^a q(\zeta) \exp \left[-i \frac{\pi}{\lambda z} a^2 \zeta \right] J_m \left(\frac{2\pi}{\lambda z} ar \sqrt{\zeta} \right) d\zeta \right|^2 \quad (3)$$

$$\Phi(z, r, \theta) = m \left(\theta + \frac{\pi}{2} \right) - \frac{2\pi}{\lambda} z - \frac{\pi r^2}{\lambda z} - \frac{\pi}{2}; \quad (4)$$

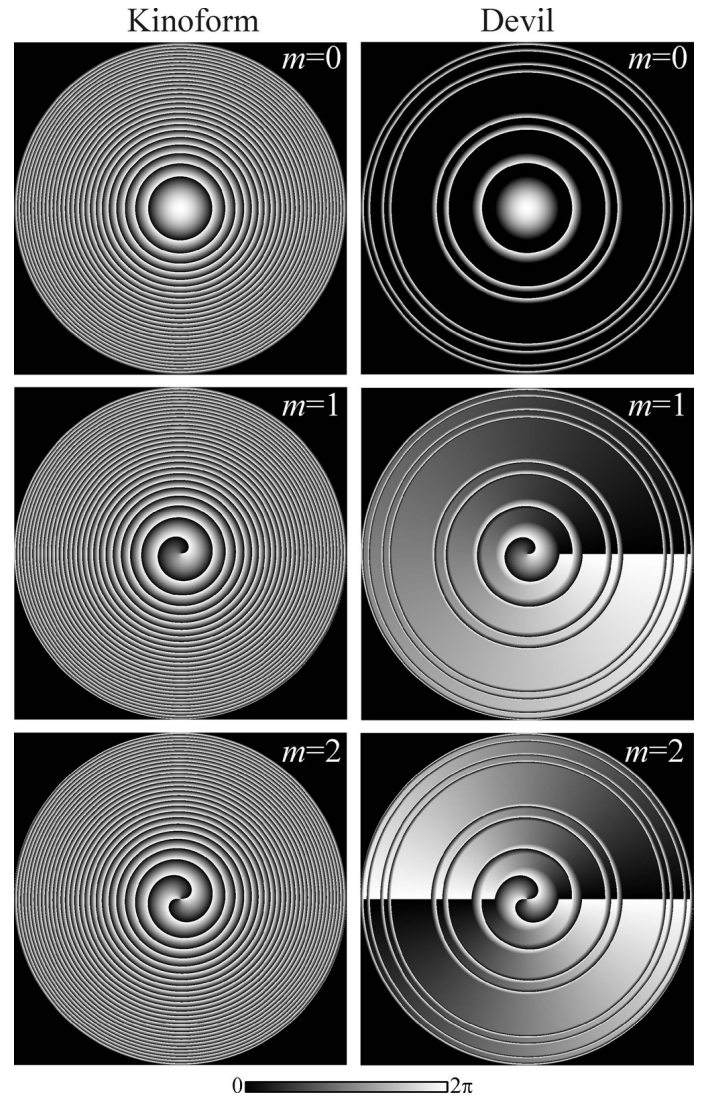


FIG. 2 Phase variation as gray levels for vortex lenses with different values for the topological charge. Left: Conventional Fresnel kinoforms; Right: DVLs ($S = 3$), with topological charges $m = 0, 1,$ and 2 .

where z is the axial distance from the pupil plane and λ is the wavelength of the plane wave. By using the above equations we have computed the irradiance provided by the DVLs in Figure 2. The results are represented in Figure 3. As expected, the axial response for the DVLs exhibit a single major focus at $f_s = a^2/2\lambda 3^S$ and a number of subsidiary focal points surrounding it, producing a focal volume with a characteristic fractal profile. Note that, for non-null values of the topological charge each focus is a vortex and a chain of doughnut shaped foci is generated. Figures 3(b) and 3(c) show the focal volume associated to the DVL with $m = 1$ and $m = 2$, respectively. We have also computed the diffraction patterns for different topological charges and verified that the diameter of the doughnut increases with the topological charge as happens with conventional vortex producing lenses [13, 14]. For comparison the pattern corresponding to conventional kinoform vortex lenses are shown in Figure 4. It can be seen that the axial position of the focus of the Fresnel kinoform vortex lens and the central lobe of the DVL focus both coincide at the normalized distance. For the DVLs we have found that the axial irradiance distributions corresponding to different values of S are self-similar, i.e., as S becomes larger an increasing number of zeros

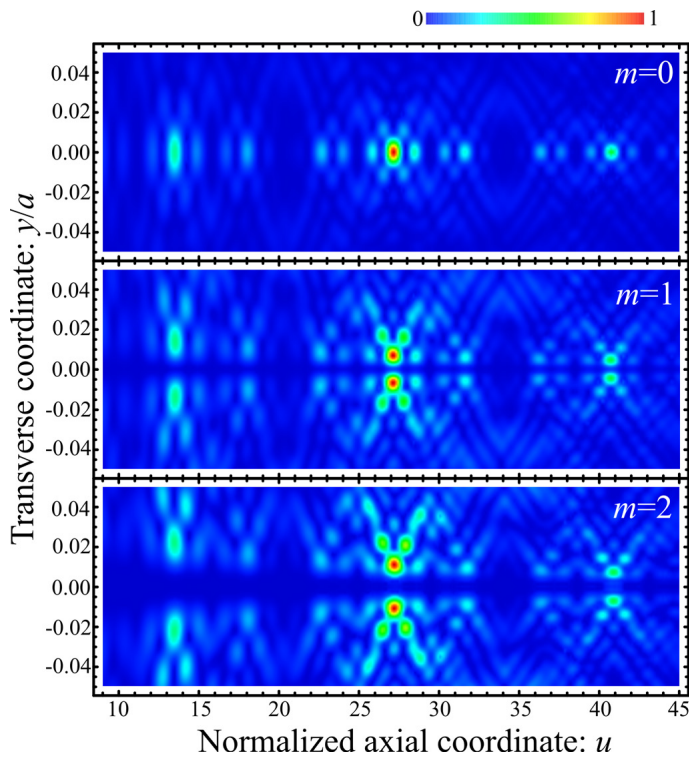


FIG. 3 Normalized irradiance contours computed for the DVLS in Figure 2. (a) $m = 0$, (b) $m = 1$, and (c) $m = 2$.

and maxima are encountered but the scaled irradiance corresponding to the DVLS of low level form the envelope of those corresponding to the upper ones. This focalization behavior, which is here demonstrated that DVLS satisfy was previously found for FraZPs and it was called *the axial scale property* in [8]. If, as it was done in this work, we express the axial irradiance in terms of the normalized axial coordinate $u = a^2/2\lambda z$, then it is easy to show that, in terms of this variable, Eq. (3) can be understood as a Fourier transform with frequency component u . Thus, from well-known properties of fractals, it is straightforward to obtain that DVLS provide a self-similar axial irradiances in the variable u .

To investigate quantitatively the degree of self-similarity of the axial irradiances provided by DVLS with different values of m , we calculated the following normalized correlation [15] between the axial irradiances, computed using Eq. (3) for $S = 3$ and different scales γ , i.e.:

$$C(\gamma) = \frac{\int_{-\infty}^{\infty} I(u) I((u - u_0)/\gamma + u_0) du}{\sqrt{\int_{-\infty}^{\infty} I^2(u) du \int_{-\infty}^{\infty} I^2((u - u_0)/\gamma + u_0) du}}, \quad (5)$$

where $u_0 = a^2/2\lambda f_S = 3^S$ is the normalized main focal distance. Note that $C(\gamma) = 1$ only when $I(u)$ satisfies the strict axial self-similar property $I(u) = I((u - u_0)/(\gamma + u_0))$, i.e., for $\gamma = 1$. Correspondingly, lower degrees of self-similarity give values of $C(\gamma)$ lower than unity. Therefore, if $C(\gamma)$ is plotted against the logarithm of the scale, some local maxima of the curve are expected to appear at $\gamma = 3^i$ with $i = 0, 1, \dots, S$. The results are shown in Figure 5. In these curves local maxima appear at $\gamma = 1, 3, 9$, and 27 . For $m = 0$ the values of the irradiance in Eq. (5) were computed along the optical axis. For $m = 1$ and $m = 2$ the irradiances were computed for fixed values of r coinciding with the maximum value of the irradiances

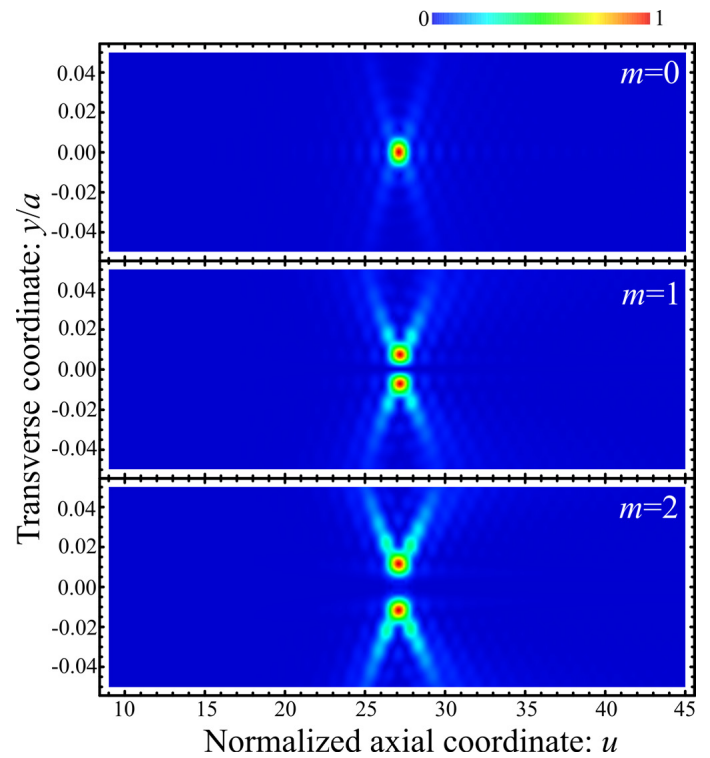


FIG. 4 Normalized irradiance contours computed for the conventional vortex lenses in Figure 2. (a) $m = 0$, (b) $m = 1$, and (c) $m = 2$.

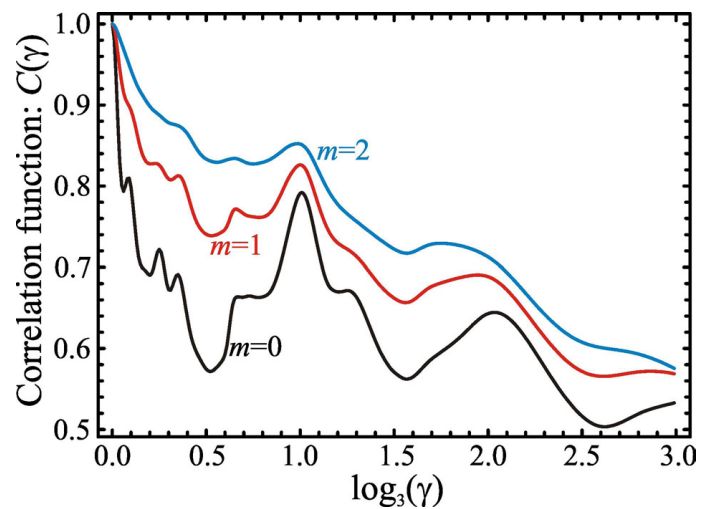


FIG. 5 Correlation function $C(\gamma)$ for the axial irradiances computed for the DVLS in Figure 2.

in Figure 3. It can be seen that the degree of self-similarity lowers for increasing m .

4 EVOLUTION OF THE ANGULAR MOMENTUM

Eq. (4) has been used to calculate the phase variations of the diffracted field from plane to plane generated by the DVLS represented in Figure 4 around the main vortices. The results are shown in Figure 6. In the animation each frame represents the form of the transverse field contours as the product of the irradiance and the phase of the wavefront. The intensities are normalized to the maximum value at each transverse plane. In this way, the relative intensity at the vortices can be directly

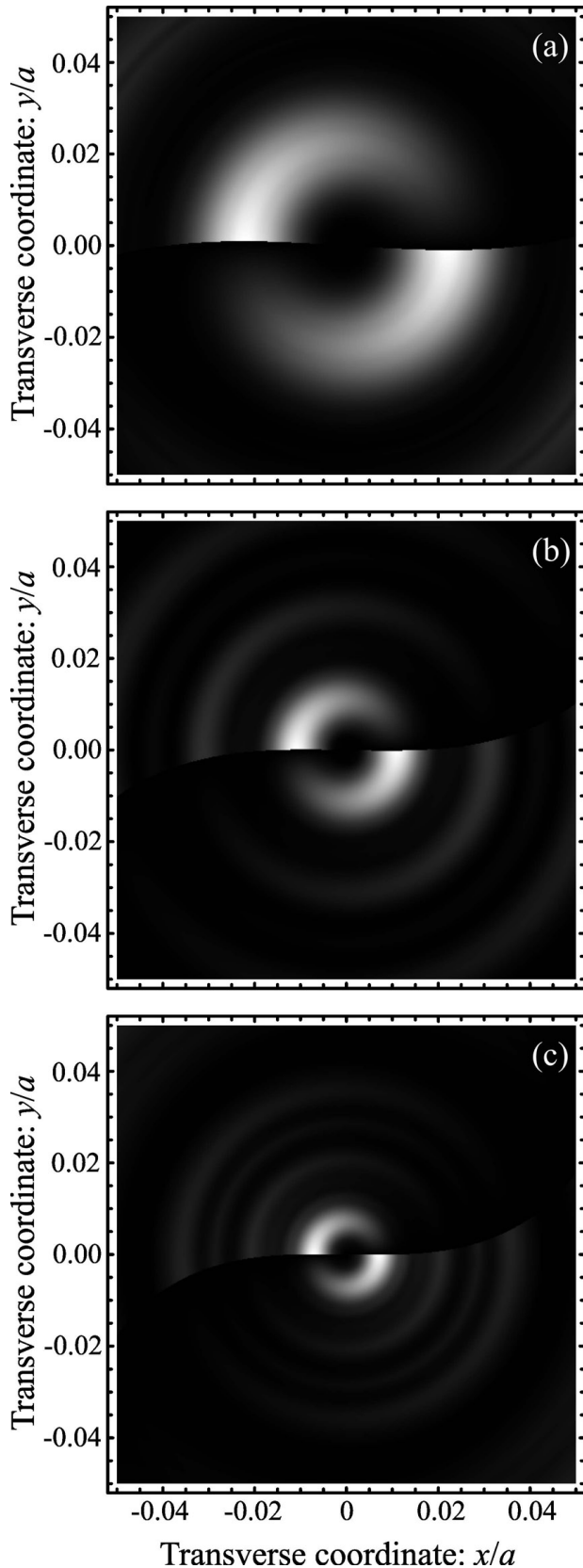


FIG. 6 Transverse field maps (as the product of the irradiance times phase) at (a) $z/f = 2$, (b) $z/f = 1$, and (c) $z/f = 2/3$, computed for the DVLs represented in Figure 2 with $S = 3$ and $m = 2$. The animation (videoseize 3.9 MB, format: gif, see Fig6.gif) shows the evolution of the vortices as they propagate through the foci in an axial interval $\Delta(z/f) = 1.71 \times 10^{-5}$.

compared. These animations show the annular form of the transverse intensity and also the phase rotation with the axial coordinate. Note that due to the form of this representation

only the changes in the phase are relevant since the intensity didn't change with time. The concentric rings are caused by constructive interferences of the different rings of the DVL. According to Eq. (4) the variation of the phase with the variable z predicts a different momentum for the different links of the chain. However, in Figure 6 these differences cannot be appreciated. The reason for this apparent paradox lies in the values of the parameters used in the calculation for this figure. In fact, for this set of parameters the derivative of the phase with respect to z of the term that depends inversely proportional to z is negligible compared to the other term depending linearly on the same variable. As a final remark on Figure 6 we mention that obviously, if the topological charge has negative sign, the rotation will be in the opposite sense.

5 CONCLUSIONS

The ability of DVLs to produce multiple vortex-tweezer has been investigated. It was found that, contrary to conventional spiral zone plate, which produces a single vortex-tweezer a DVL generates a delimited chain of vortices that are axially distributed. The distances between the links of the chain depend on the level S of the Cantor function and the radii of the doughnuts increase with the topological charge. The evolution of the irradiance along the propagation axis reproduces the fractality of the pupil. The orbital angular momentum associated to each link on the chain is also mainly dependent on the topological charge and it can be nearly independent of its axial location.

The particular focal volume provided by DVLs could be profited as versatile and very efficient optical tweezers since in addition to exert a torque on micrometer-scale objects having a high refraction index, it can also trap the low-index particles in the zero intensity region of the doughnut.

6 ACKNOWLEDGMENTS

We acknowledge the financial support from Ministerio de Ciencia e Innovación (DPI2008-02953 and TRA2009-0215), Spain. We also acknowledge the support from Generalitat Valenciana (PROMETEO2009-077 and ACOMP/2010/052) and from Universidad Politécnica de Valencia (PAID-05-09 and PAID-06-08), Spain. L. Remón acknowledges a fellowship of "Fundación Cajamurcia", Spain.

References

- [1] F. S. Roux, "Distribution of angular momentum and vortex morphology in optical beams" *Opt. Commun.* **242**, 45-55 (2004).
- [2] G. Gbur, and T. D. Visser, "Phase singularities and coherence vortices in linear optical systems" *Opt. Commun.* **259**, 428-435 (2006).
- [3] A. I. Bishop, T. A. Nieminen, N. R. Heckenberg, and H. Rubinsztein-Dunlop, "Optical application and measurement of torque on microparticles of isotropic nonabsorbing material" *Phys. Rev. A* **68**, 033802 (2003).

- [4] K. Ladavac, and D. Grier, "Microoptomechanical pumps assembled and driven by holographic optical vortex arrays" *Opt. Express* **12**, 1144-1149 (2004).
- [5] W. M. Lee, X. C. Yuan, and W. C. Cheong, "Optical vortex beam shaping by use of highly efficient irregular spiral phase plates for optical micromanipulation" *Opt. Lett.* **29**, 1796-1798 (2004).
- [6] S. H. Tao, X.-C. Yuan, J. Lin, and R. Burge, "Sequence of focused optical vortices generated by a spiral fractal zone plates" *Appl. Phys. Lett.* **89**, 031105 (2006).
- [7] W. D. Furlan, F. Giménez, A. Calatayud, and J. A. Monsoriu, "Devil's vortex-lenses" *Opt. Express* **17**, 21891-21896 (2009).
- [8] G. Saavedra, W. D. Furlan, and J. A. Monsoriu, "Fractal zone plates" *Opt. Lett.* **28**, 971-973 (2003).
- [9] J. A. Monsoriu, G. Saavedra, and W. D. Furlan, "Fractal zone plates with variable lacunarity" *Opt. Express* **12**, 4227-4234 (2004).
- [10] F. Giménez, J. A. Monsoriu, W. D. Furlan, and A. Pons, "Fractal Photon Sieves" *Opt. Express* **14**, 11958-11963 (2006).
- [11] J. A. Monsoriu, W. D. Furlan, G. Saavedra, and F. Giménez, "Devil's lenses" *Opt. Express* **15**, 13858-13864 (2007).
- [12] D. R. Chalice, "A characterization of the Cantor function" *Amer. Math. Monthly* **98**, 255-258 (1991).
- [13] G. A. Swartzlander, Jr, "Peering into darkness with a vortex spatial filter" *Opt. Lett.* **26**, 497-499 (2001).
- [14] J. E. Curtis, and D. Grier, "Structure of Optical Vortices" *Phys. Rev. Lett.* **90**, 133901 (2003).
- [15] J. A. Monsoriu, C. J. Zapata-Rodriguez, and W. D. Furlan, "Fractal axicons" *Opt. Commun.* **263**, 1-5 (2006).